Materials Today Bio 23 (2023) 100830

Contents lists available at ScienceDirect

Materials Today Bio

journal homepage: www.journals.elsevier.com/materials-today-bio

Hypotrochoidal scaffolds for cartilage regeneration

Kenny A. van Kampen [a], Elena Olaret [b], Izabela-Cristina Stancu [b], Daniela F. Duarte Campos [c], Horst Fischer [d], Carlos Mota [a], Lorenzo Moroni [a,*]

[a] Department of Complex Tissue Regeneration, MERLN Institute for Technology-Inspired Regenerative Medicine, Maastricht University, Universiteitsingel 40, 6229ER, Maastricht, the Netherlands
[b] Advanced Polymer Materials Group, University Politehnica of Bucharest, 1-7 Gh. Polizu Street, 011061, Bucharest, Romania
[c] Bioprinting & Tissue Engineering Group, Center for Molecular Biology Heidelberg (ZMBH), Heidelberg University, Germany
[d] Department of Dental Materials and Biomaterials Research, RWTH Aachen University Hospital, Aachen, Germany

ARTICLE INFO

Keywords:
Additive manufacturing
G-code design
Cartilage tissue engineering
Dynamic culture

ABSTRACT

The main function of articular cartilage is to provide a low friction surface and protect the underlying subchondral bone. The extracellular matrix composition of articular cartilage mainly consists of glycosaminoglycans and collagen type II. Specifically, collagen type II fibers have an arch-like organization that can be mimicked with segments of a hypotrochoidal curve. In this study, a script was developed that allowed the fabrication of scaffolds with a hypotrochoidal design. This design was investigated and compared to a regular 0–90 woodpile design. The mechanical analyses revealed that the hypotrochoidal design had a lower component Young's modulus while the toughness and strain at yield were higher compared to the woodpile design. Fatigue tests showed that the hypotrochoidal design lost more energy per cycle due to the damping effect of the unique microarchitecture. In addition, data from cell culture under dynamic stimulation demonstrated that the collagen type II deposition was improved and collagen type X reduced in the hypotrochoidal design. Finally, Alcian blue staining revealed that the areas where the stress was higher during the stimulation produced more glycosaminoglycans. Our results highlight a new and simple scaffold design based on hypotrochoidal curves that could be used for cartilage tissue engineering.

1. Introduction

Articular cartilage is an avascular tissue that is located in the joints [1]. The main function of cartilage is to protect the underlying subchondral bone from compressive loads and to provide a low-friction surface [2]. Injury or damage to cartilage can hamper this function and could lead to osteoarthritis [3]. Unfortunately, articular cartilage has a poor regenerative capacity due to the avascular and scarce cell density nature within the tissue [4]. Chondrocytes are the main cell population in articular cartilage and are responsible for synthesizing the extracellular matrix (ECM) [5]. The ECM of articular cartilage mainly consists of collagen type II, aggrecan and other proteoglycans [6]. The organization of the ECM is important in cartilage, specifically the collagen type II fibers have a particular organization which helps to improve the mechanical properties [7]. Cartilage is characterized by three distinct zones; (1) the superficial zone which has collagen fibers oriented parallel to the surface, (2) the intermediate zone where there is no predominant orientation and (3) the deep zone which shows a high orientation with fibers perpendicular to the underlying bone [8]. Each of these zones have a different composition in ECM and cell density [9], which contributes to the unique properties of articular cartilage.

The organization of the collagen type II fibers could be mathematically described with arches or arch-like structures. A hypotrochoid is one of type of curve that could be used to describe an arch-like structure. This geometric curve is generated by tracing a point that is linked to a smaller circle, which is rolling inside a larger circle [10]. The hypotrochoidal curve is used to describe in a simplified way the satellite orbits around a planet in a solar system [11] and can be drawn using a tool called Spirograph [12]. The hypotrochoid is characterized by a closed outer surface with the outer shape being round in most cases. Depending on the parameters used, the hypotrochoidal curve can have a dense outer part with lines running parallel to the circle. These parallel

Abbreviations: ECM, extracellular matrix; AM, Additive manufacturing; FDM, Fused deposition modelling; PCL, Poly(ε-caprolactone); CAD, computer assisted design; GAG, glycosaminoglycan.

* Corresponding author.
E-mail address: l.moroni@maastrichtuniversity.nl (L. Moroni).

https://doi.org/10.1016/j.mtbio.2023.100830
Received 11 June 2023; Received in revised form 30 September 2023; Accepted 9 October 2023
Available online 14 October 2023
2590-0064/© 2023 The Authors. Published by Elsevier Ltd. This is an open access article under the CC BY-NC-ND license (http://creativecommons.org/licenses/by-nc-nd/4.0/).

lines, in combination with a more porous inner core with lines that run perpendicular to the surface of the circle, make it an interesting geometry that can be used to mimic cartilage ECM architecture. The generated arch-like structure resembles the collagen type II organization, especially if a segment on the top of the curve is taken. In addition, the complex arch-like structure should be able to distribute the forces through the whole scaffold more evenly [13].

Additive manufacturing (AM) techniques such as fused deposition modeling (FDM) and bioprinting have been widely used to fabricate scaffolds for cartilage regeneration [14]. The main advantage of AM techniques is the possibility to tailor the design and porosity of the scaffold [15]. Many scaffold fabrication approaches focus on matching the mechanical properties of native cartilage with a common strategy of changing geometry or by adding materials to the scaffold [16]. While techniques such as FDM do pose the ability to produce complex shapes, in most cases a woodpile design is used where each layer is a composition of parallel running lines stacked in different angles with each layer [17]. Some efforts have been made to introduce complexity in the design, such as introducing gradients by increasing the spacing between the fibers in each layer [18] or using different periodic infilling patterns [19]. However, none of these studies take a biomimicking approach from both a morphological and a mechanical point of view in the design of the scaffold. This could both be achieved by using a hypotrochoidal design.

In this study, we propose a new strategy to fabricate additive manufactured scaffolds with a hypotrochoidal pore network architecture. The mechanical properties of several hypotrochoidal designs were compared to a classical 0–90 woodpile structure. To reduce the influence of material properties Polycaprolactone (PCL) was chosen as inert biomaterial to study the effect of the architecture. In addition, a finite element model was used to simulate the stress distribution through the scaffold. Finally, the effect of the hypotrochoidal design on cellular behavior was studied in both static and dynamic culture conditions.

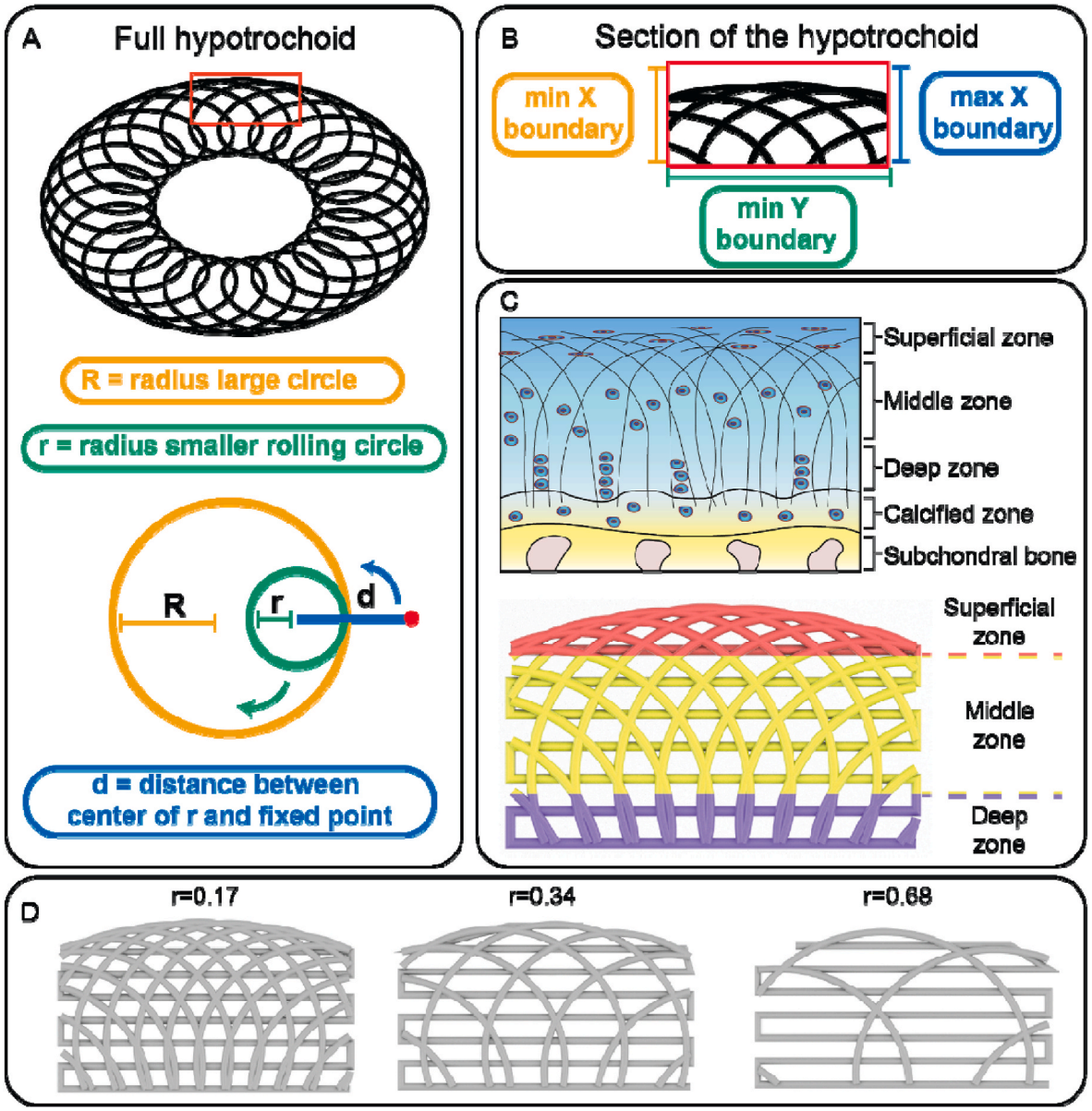

Fig. 1. Nomenclature of the hypotrochoidal scaffold (A). Section of the hypotrochoidal scaffold (B). Different zones of the hypotrochoidal scaffold representing the different zones in articular cartilage, the fiber diameter in the scaffold is in the micron range while the bundles of collagen fibers is in the sub-micron range (C). Rendered images of the three tested designs with different r values (D).

2. Results

2.1. Scaffold fabrication and morphology

The nomenclature and fabrication parameters are shown in Fig. 1. Briefly, the full hypotrochoid was sectioned by boundaries to mimic the collagen type II alignment. The scaffolds were fabricated through FDM after digital sectioning. The final scaffolds were divided in three distinct zones based on literature, deep (25 %), middle (55 %) and superficial zone (20 %) (supplementary information, Fig. S1) [20]. For the hypotrochoidal designs, parameters R, d and the boundaries were kept the same while r varied between 0.17 and 0.68. As control a 0–90 design was compared to the hypotrochoidal designs.

As seen from both stereomicroscopy and micro-CT images the hypotrochoidal designs were successfully fabricated (Fig. 2). The hypotrochoidal scaffolds had a curved top surface due to the way a hypotrochoid was generated. The meandering layers between the hypotrochoidal layers served as a support during the fabrication process. Signs of fiber collapse were noted in the designs that were more porous, due to the lack of support for the fabricated fiber that had to span in air multiple millimeters (Fig. S2). The pores in all of the tested designs were interconnected. In the hypotrochoidal design, a gradient in pore size was observed with the smallest pores in the superficial zone and the largest pores in the deep zone. The volumetric analyses revealed that the solid scaffold volume of the hypotrochoidal design increased from 40.0 ± 0.4 mm^3 to 65.0 ± 2.4 mm^3 with a lower r value (r = 0.68 and r = 0.17 respectively) (Table 1). A similar observation was made with the available surface area, increasing from 636.8 ± 14.5 mm^2 to 919.3 ± 79.7 mm^2 in the r = 0.68 and r = 0.17 samples, respectively, while the surface area to volume ratio remained similar between the hypotrochoidal conditions. The 0–90 structure was similar in volume to the r = 0.68 scaffold (42.4 ± 1.2 mm^3 and 40.0 ± 0.4 mm^3 respectively) while having a higher surface area (722.0 ± 40.3 mm^2 and 636.8 ± 14.5 mm^2 respectively). The 0–90 structure, however, showed a higher surface area to volume ratio compared to the hypotrochoidal designs. The curvature of the different designs was shown in Table 1 with minimal differences in radius between the scaffolds. The curvature for the

Table 1
Volumetric micro-CT data of the different tested designs. Each condition contained n = 3 samples. Values represent average ± standard deviation.

Sample	Scaffold Volume (mm^3)	Surface area (mm^2)	Surface area/ Volume (1/mm)	Superficial zone radius (mm)
r = 0.68	40.0 ± 0.4	636.8 ± 14.5	15.9 ± 0.5	13.32
r = 0.34	61.9 ± 3.1	804.7 ± 114.8	16.3 ± 1.3	13.66
r = 0.17	65.0 ± 2.4	919.3 ± 79.7	14.2 ± 1.3	13.83
0–90	42.4 ± 1.2	722.0 ± 40.3	17.0 ± 0.5	13.83

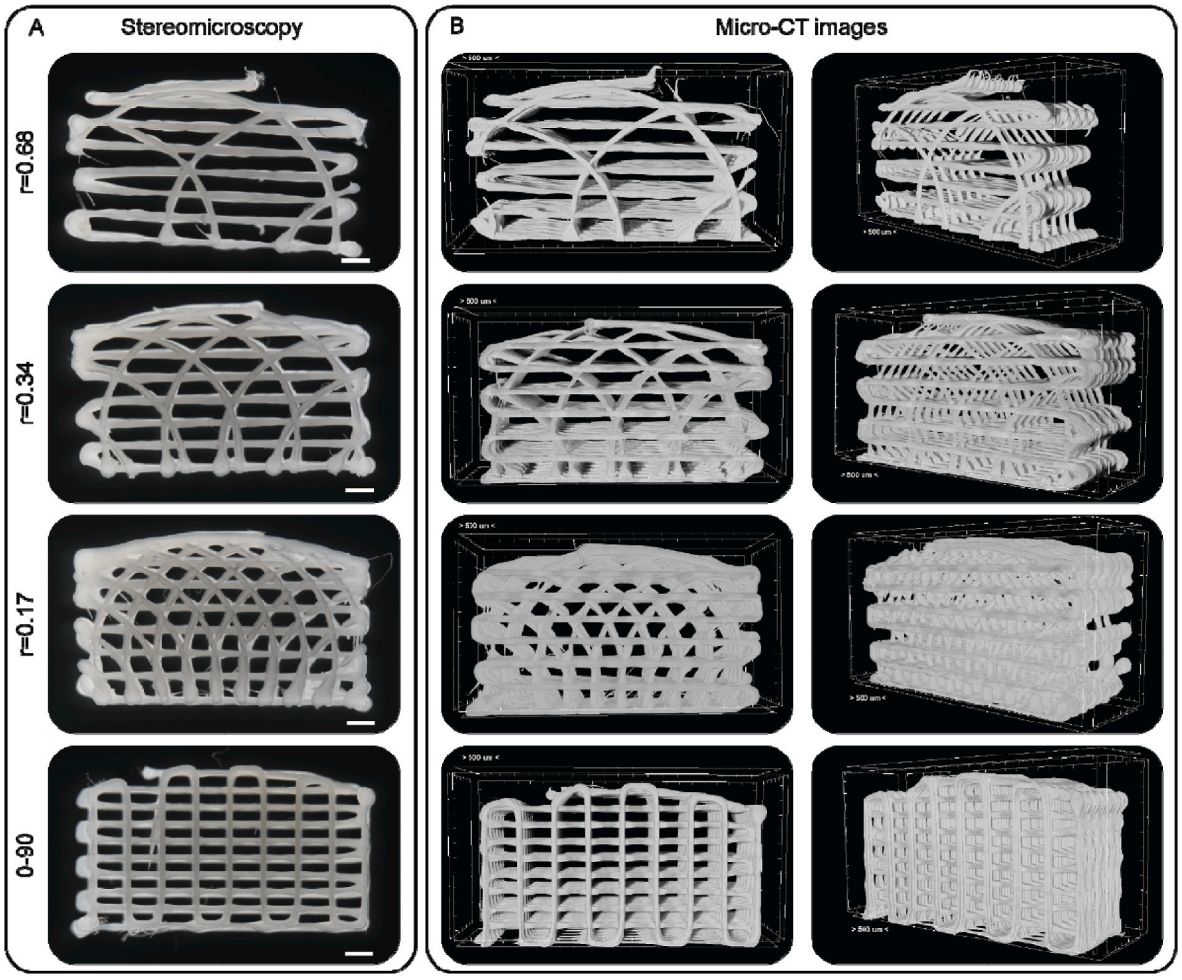

Fig. 2. Overview of the tested designs. (A) Stereomicroscopy images of the frontal view of the tested designs. (B) The micro-CT images of the scaffolds, the frontal view in the left panels and the perspective view in the right panels. Scale bar represents 500 μm.

0–90 structure was set equal to the r = 0.17 design.

2.2. Mechanical testing and finite element modeling

The mechanical properties of the hypotrochoidal designs were tested via compression and fatigue tests. CAD models of the scaffolds were also imported in finite element software and a compression test was simulated. The compression tests revealed that the Young's modulus in the 0–90 structure was significantly higher compared to the r = 0.17 hypotrochoidal designs (21.0 ± 1.8 MPa and 14.1 ± 1.8 MPa, respectively) (Fig. 3A). In addition, the increase in r caused a decrease in Young's modulus from 14.1 ± 1.8 MPa to 1.4 ± 0.1 MPa for r = 0.17 and r = 0.68 samples respectively. The differences in yield strain between hypotrochoidal designs was small ranging from 7.9 ± 0.0 % and 11.0 ± 2.6 % strain in the r = 0.34 and r = 0.68 respectively (Fig. 3B). The yield strain in the 0–90 design was significantly lower at 4.2 ± 0.4 % compared to the hypotrochoidal designs. The yield strength in the hypotrochoidal designs decreased significantly with the increase in r from 36.9 ± 2.2 N to 5.9 ± 2.6 N (Fig. 3C). The 0–90 design had a yield strength that was significantly different, between the r = 0.17 and r = 0.34 design (21.8 ± 3.6 N, 36.9 ± 2.2 N and 10.9 ± 0.6 N respectively). The toughness in the r = 0.17 was significantly higher at 0.035 ± 0.001 N mm^2 compared to the other tested designs at 0.008 ± 0.002 N mm^2, 0.011 ± 0.001 N mm^2 and 0.006 ± 0.004 N mm^2 for the 0–90, r = 0.34 and r = 0.68 design respectively (Fig. 3D). The stress strain curves showed that the stress in 0–90 structure after the yield point decreased, while in all of the hypotrochoidal designs kept increasing (Fig. 3E). Time lapsed snapshots showed that near the yield point 0–90 structure buckled in the middle of the scaffold and the square pore shape became rhomboidal (Fig. 3F, supplemental video S1). However, the hypotrochoidal designs did not show this behavior. Instead, the top pores collapsed while the bottom pores remained intact, even far beyond the yield point (Fig. S3). This was also confirmed during the compression test and micro-CT analyses where the 0–90 structure buckled in the top half of the scaffold, while the hypotrochoidal designs collapsed inward (Fig. S4). Even at 25 % strain the bottom part of the hypotrochoidal scaffolds showed interconnected pores (Fig. S5).

A finite element model simulated up to 10 % strain on the scaffolds with increments of 2 % was performed. The model revealed that the vertical fibers in the 0–90 design endured the highest von Mises stress while the horizontal fibers were unaffected (Fig. S6). The displacement in the scaffold was evenly distributed from the bottom to the top of the scaffold. The stress distribution in the hypotrochoidal designs was improved compared to the 0–90 design, where the arches distribute the stress throughout the scaffolds and even in the meandering layer there was an increase in von Mises stresses. The highest stress was found in the superficial part of the scaffold (Fig. S6).

Based on the results from the compression test, a fatigue test of 100 cycles at 1 Hz with a fixed 2.5 % strain was performed. The data from the fatigue test showed that the hysteresis loop was the steepest in the 0–90 design compared to the hypotrochoidal designs (Fig. 4A). The percentage energy lost per cycle, however, was significantly higher in the r = 0.34 and the r = 0.68 designs compared to r = 0.17 and 0–90 designs (4.7 ± 0.5 %, 6.0 ± 0.5 % and 3.8 ± 0.5 % respectively) (Fig. 4B). The peak force in all of the samples decreased by a small amount in the initial cycles and stabilized after that initial decrease (Fig. 6C). The average peak force in the 0–90 structure was the highest stabilizing around 12 N while in the r = 0.68 it was the lowest at around 2 N.

2.3. Dynamic cell culture

Cell culture experiments were performed on the r = 0.17 design and the 0–90 woodpile structure to assess the cellular behavior on the hypotrochoidal design. Initially the r = 0.34 design was tested, however after 28 days of static culture the scaffolds' pores remained open, resulting in low GAG synthesis (Fig. S7), despite cell proliferation and good adhesion (Fig. S8). Therefore, r = 0.17 design was chosen since the pore size of the r = 0.34 and the r = 0.68 design were too large and would likely not be closed by sufficient regenerated tissue after the culture period. The fraction of the pore volume based on the micro-CT data in both the 0–90 woodpile structure and the r = 0.17 design was similar for each zone (Fig. 5A, Table S1). The scaffolds were seeded with ATDC5 cells, which are known as hypertrophic chondrocytes, and some of the scaffolds were transferred to a bioreactor after 7 days. A day 1 DNA quantification was done to asses if the scaffolds contained similar amount of cells. A dynamic culture was performed by applying a mechanical stimulation for 2 h every day at 1 Hz and 2.5 % strain until 28 days. The DNA in the samples was normalized against the pore volume. There was no difference found between the amount of DNA found at day 1 between the 0–90 woodpile and r = 0.17 design (13.5 ± 1.3 ng and 12.7 ± 1.2 ng respectively). A division was made based on the fraction of the pore volume found in each zone with the assumption that the cells were equally distributed throughout the scaffold (Fig. S9). The dynamic stimulation increased the DNA per pore volume in the r = 0.17 samples from 4.6 ± 1.0 μg/mm^3 to 5.9 ± 0.4 μg/mm^3 respectively while there was a slight decrease observed in the 0–90 woodpile design from 6.2 ± 1.3 μg/mm^3 to 5.8 ± 0.8 μg/mm^3 (Fig. 5B, Table S2). Between the tested designs it was noted that the DNA per pore volume was approximately similar. The GAG/DNA per pore volume remained similar in all of the tested conditions (Fig. 5C). Dynamic stimulation did increase the collagen/DNA per pore volume in the 0–90 woodpile design (15.6 ± 2.2 ng/μg/mm^3 and 16.7 ± 0.8 ng/μg/mm^3 respectively), while in the r = 0.17 design it remained similar. Total DNA, GAG, and Collagen increased in dynamic culture conditions compared to static culture, even more so in the hypotrochoidal scaffold design than the 0–90 woodpile design (Table S2). Yet, comparable values were observed if the values were corrected by the available surface area instead of the pore volume (Fig. S10).

Alcian blue staining revealed that there was GAG deposition through the entire scaffold in all of the conditions (Fig. 6). More pores in the 0–90 woodpile static condition seemed to be open compared to the dynamically stimulated samples. The intensity of the staining however was stronger in the static samples. The majority of the pores in r = 0.17 hypotrochoidal design were open in both the static and dynamic samples, except for the smaller pores that were mainly located in the superficial zone of the scaffold. The r = 0.17 dynamically stimulated samples showed darker areas with more GAG deposition that correlated with areas that should have received less stress during the culture located in the deep zone of the scaffold.

Fluorescent images from the dynamic culture revealed a reduced collagen type X expression in the hypotrochoidal scaffolds compared to the 0–90 woodpile design (Fig. 7). Combining the experimental data with the computational data from the finite element model revealed that in both scaffolds' design the amount of collagen type X was higher in the areas where there was more von Mises stress. Interestingly, in the hypotrochoidal design higher collagen type II expression was observed in the areas where the von Mises stress was increased, whereas there was almost no collagen type II expression in the 0–90 woodpile design. In the static conditions there was no collagen type II expression observed (Fig. S11). The expression of collagen type X was comparable throughout the scaffolds.

3. Discussion

In this study, a scaffold was created from a hypotrochoidal deposition pattern. The morphology of the hypotrochoidal scaffold resembled that of the collagen fiber architecture in articular cartilage [8a]. In addition, micro-CT analyses revealed that the hypotrochoidal scaffold had a fully interconnected pore network, which is necessary to have a proper access to nutrients [21]. The mechanical tests showed that the hypotrochoidal design had a lower Young's modulus while having a significantly higher yield strain and higher toughness. Finite element

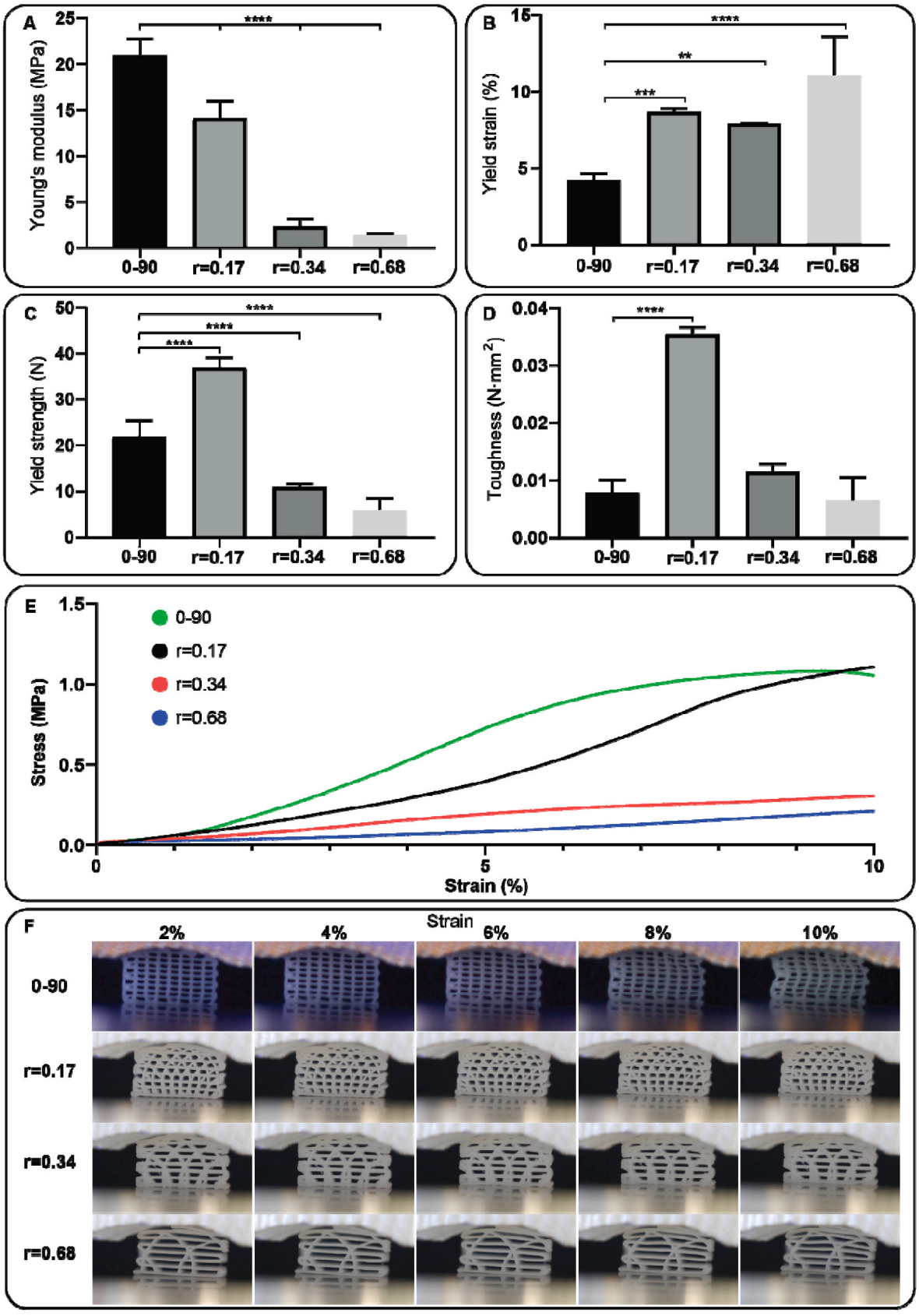

Fig. 3. Compression test of the investigated designs: (A) Young's modulus, (B) yield strain, (C) yield strength, (D) toughness, (E) representative stress strain curve, and (F) time-lapsed snapshots during the compression test. Each condition contained n = 5 samples and values represent average ± standard deviation. Statistical significance: *p < 0.05, **p < 0.01, ***p < 0.005, ****p < 0.0001.

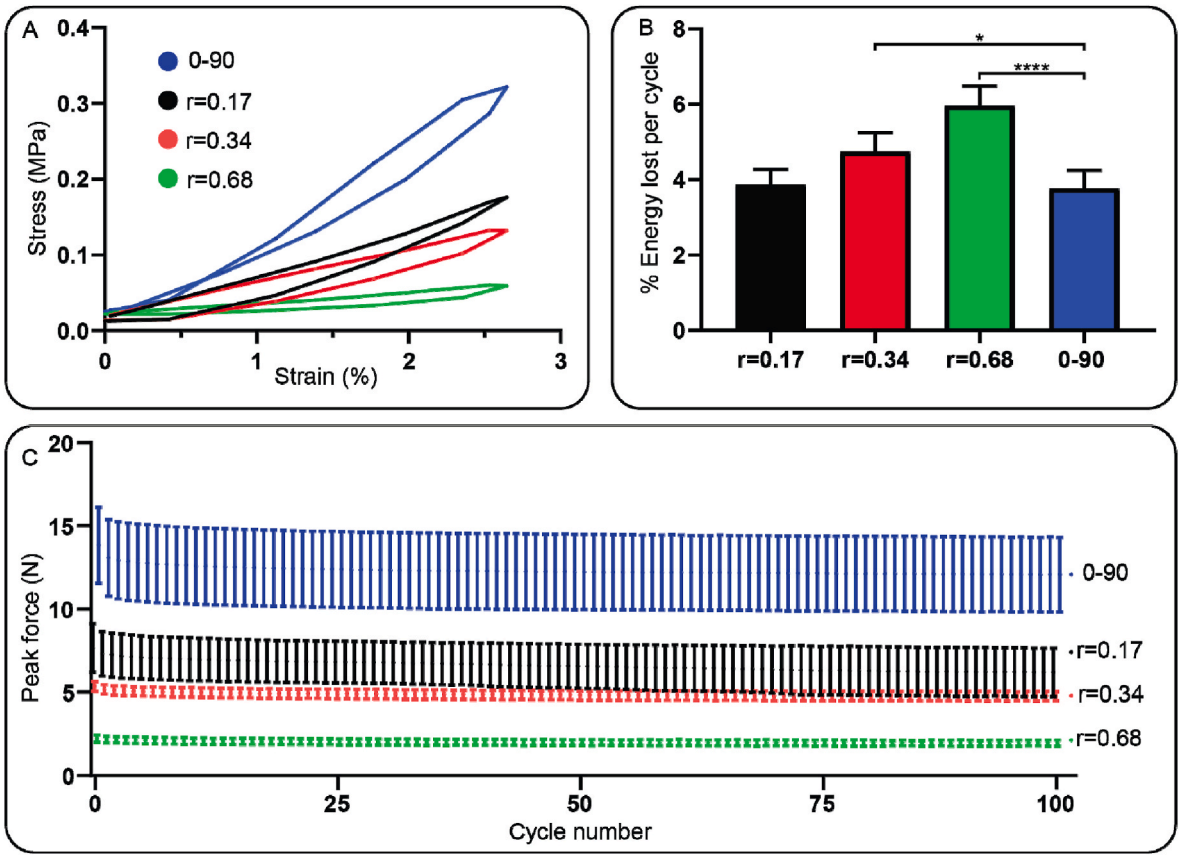

Fig. 4. Fatigue test data with a frequency of 1 Hz until a strain of 2.5 %. (A) Hysteresis loop of a single cycle during the fatigue test. (B) Average energy lost per cycle during the fatigue test. (C) Average peak force of each cycle. Each condition contained n = 5 samples and values represent average ± standard deviation. Statistical significance: *p < 0.05, **p < 0.01, ***p < 0.005, ****p < 0.0001.

model demonstrated that the stress distribution was improved with the hypotrochoidal design compared to the 0–90 woodpile structure. Further mechanical analysis from the fatigue test revealed that the hypotrochoidal design dissipated more energy per compression cycle. Finally, the dynamic culture demonstrated that the hypotrochoidal design had improved collagen type II deposition. Hence, the hypotrochoidal design could potentially be used for cartilage tissue regeneration.

The micro-CT analysis revealed that there was a pore gradient in the hypotrochoidal design, where the smallest pores resided in the top part of the scaffold and the largest pores in the bottom. This gradient can be beneficial since the structure of articular cartilage is heterogeneous, resulting in different regions of cartilage having a different range in mechanical properties [9]. Due to how a hypotrochoid is generated, the superficial zone of the scaffold always has a curved surface. The surface of healthy articular cartilage, however, is not perfectly round and is almost flat [22]. A solution to this could be to have R at least a factor 1000 bigger compared to r. This is also evident from equation (3), when R becomes so much larger the radius of the zone increases. This would approximate a flat surface while still creating a hypotrochoidal design. The hypotrochoidal design consists of parameters r, R and d. These parameters have no constrains and therefore give an infinite amount of possible hypotrochoidal designs. A programmed macro-function can offer the possibility to simulate what kind of final hypotrochoidal design is generated with the given parameters. Another option to investigate could be to edit the formula to generate a different hypotrochoidal pattern. An example of this could be to add another sine function within the equation for the Y-coordinate to create a concave surface that could be useful for other type of cartilages, for example similar to the meniscus [23]. The chondrocytes in the superficial zone are responsible for the synthesis of superficial zone protein and hyaluronan that acts as a lubricant [24]. Due to the "circular" design of the hypotrochoid, it creates fibers along the superficial surface, which in turn could decrease the friction when sliding against the other joint. Yet, as the hypotrochoidal curve is a closed curve, the hypotrochoidal design always lead to a non-porous surface. Therefore, adding a single layer of a woodpile structure could be a strategy to introduce some porosity in the surface, which may facilitate the migration of cells to the surface of the scaffold to secrete superficial zone protein. In addition, mechanical stimulation improved hyaluronan synthesis, which could further decrease the friction in the scaffold [25]. As the relatively rough surface of PCL filaments could affect the lubricity of the scaffold. There have also been attempts to recreate the zonal architecture, but these tend to have discrete layers to create each zone of articular cartilage, as opposed to the hypotrochoidal design that utilizes a continuous arch-like gradient [26]. Other scaffolds that have been developed with a continuous gradient are created through different conventional fabrication methods like freeze drying and porogen leaching, which are also known to have several drawbacks in terms of pore interconnectivity, nutrient diffusion, and control of mechanical properties, ultimately resulting in poor cartilage regeneration [27].

It was noted that the surface area to volume ratio in the hypotrochoidal design was lower compared to the 0–90 woodpile structure. An explanation for this could be that the fibers in the 0–90 design have the least amount of overlap in fibers due to a fiber angle of 90°, while the fiber angle in the hypotrochoidal design vary with every fiber. Having a lower surface area to volume ratio could interfere with transportation of nutrients and vasculature [28]. However, for cartilage this could be less important since it is avascular and relies on nutrients through diffusion [29].

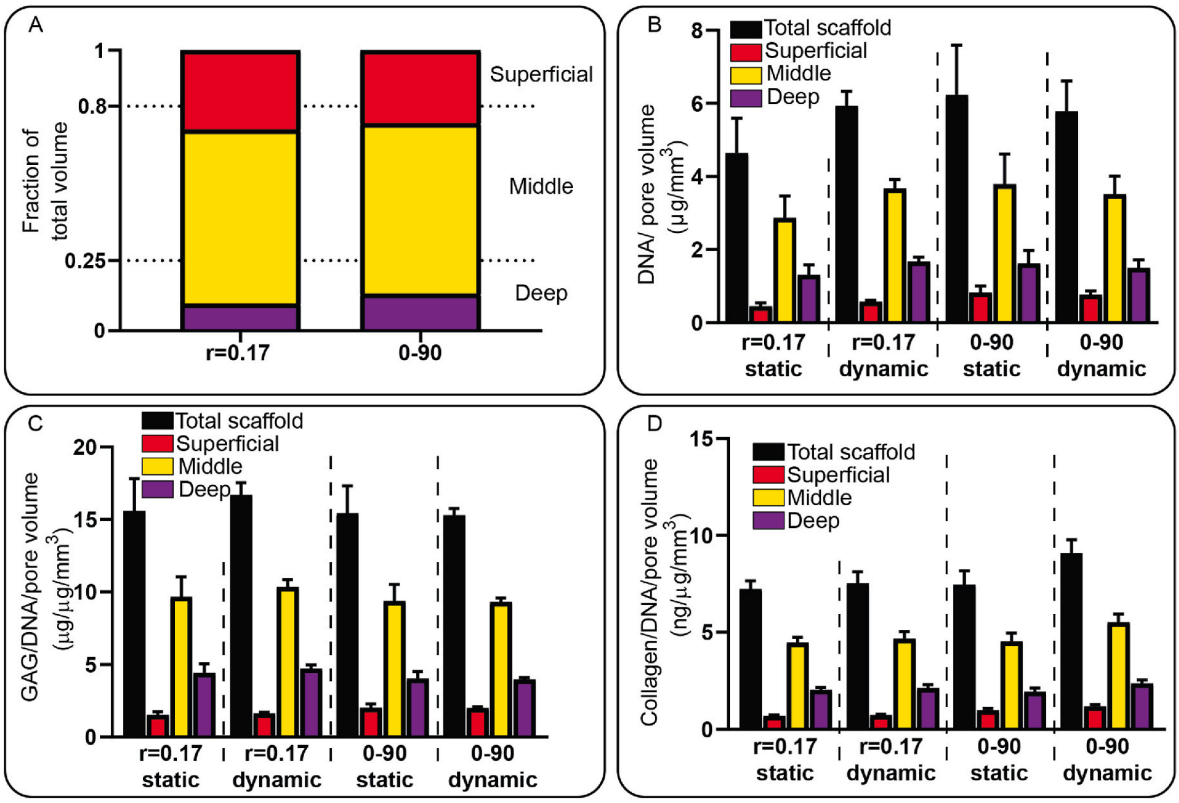

Fig. 5. DNA, GAG and collagen analyses of the tested scaffolds after 28 days of culture. (A) Volumetric analyses of the pore volume as a fraction of the total volume. (B) DNA content normalized against the pore volume. (C) GAG per DNA content normalized against the pore volume. (D) Collagen per DNA content normalized against the pore volume. Each condition contained n = 3 samples and values represent average ± standard deviation.

The mechanical properties for a tissue such as cartilage are important [30]. The Young's modulus of articular cartilage ranges from 10.6 to 18.6 MPa in the ankle joint to 5,5–11.8 MPa in the knee [31]. Specifically the r = 0.17 design resulted within this range with an average of 14.1 MPa while the 0–90 woodpile design was slightly above the maximum range with 21 MPa. Even though the 0–90 woodpile structure is stiffer, it can absorb less energy before permanently deforming as was shown by the compression test. The contribution of the arches in the hypotrochoidal design could be the reason why the 0–90 woodpile design is less tough and stiffer. The arch architecture of the hypotrochoidal design can distribute the force through the scaffolds, as was shown in the finite element models. Similar findings from Chen et al. showed that a pillar design caused a higher stress more focused on the pillars compared to an octet design with more curved features [32]. The arch architecture in the hypotrochoidal design also showed that the collapse behavior was different. While the vertical fibers in the 0–90 woodpile structure buckled, the hypotrochoidal scaffold collapsed gradually, with the superficial zone collapsing before the deeper zone. Similar to articular cartilage, after impact the superficial zone is the first zone to receive permanent damage [33]. Besides compressive forces, articular cartilage is also subjected to shear forces [34]. The hypotrochoidal design could prove beneficial as it is known that arches can distribute the shear forces through the entire structure [35]. Another observation that was made is that the energy lost per cycle in the fatigue test was higher in the r = 0.34 and r = 0.68 hypotrochoidal design compared to the 0–90 woodpile structure, indicating that having less arches in the scaffold resulted in a higher energy loss. It is reported that articular cartilage behaves as an elastic material during hysteresis, with a relative energy loss of 28 % [36]. The same study also found that a higher energy loss is also linked to cartilage damage. All the tested designs were below 10 % energy loss, which is well below the relative energy loss in articular cartilage. This value can change however, depending on the magnitude of the strain applied [37]. A 2.5 % strain for the dynamic culture was chosen based on the yield strain the 0–90 woodpile design had. The physiological relevant strain for articular cartilage in humans is 10 % or more [38], which is what could be achieved with the r = 0.68 design. Other options to improve this could involve changing the material or further exploring other hypotrochoidal designs.

GAG content is important for cartilage as it retains the water in the cartilage that can act as a lubricant [39]. Our results showed that the GAG content per DNA remained similar in all of the conditions. It is important to note that the GAG content from the biochemical assay is performed on the entire scaffold, averaging the results from all the zones. This is rather a technical limitation of extracting the tissue on such a small scale without accidently removing parts of or adding unwanted parts of interest. The division of the zones was based on the micro-CT analyses with the assumption that the cells were distributed equally through the scaffolds. However, it could be that local areas that experienced more stress can contain higher amounts of GAG. This was demonstrated by histological analysis where certain areas were darker for Alcian Blue staining, thus possibly containing more GAGs. Specifically in the deeper zone of the hypotrochoidal scaffold, the intensity of the Alcian blue staining was higher. This correlates with a native hyaline cartilage tissue where GAG content is higher in the deeper zone compared to the middle and superficial zone [9,40], Possibly due to GAG content being linked to improved mechanical properties and its deposition increased during mechanical loading [41]. Similar observations could be made for collagen content quantification, as also the collagen content is different for each zone with the highest amount of collagen found in the superficial surface [5]. The total collagen content was increased with the dynamic stimulation in the 0–90 woodpile structure. While the dynamic stimulation had no effect on the hypotrochoidal design. Examining immunostaining, however, revealed that

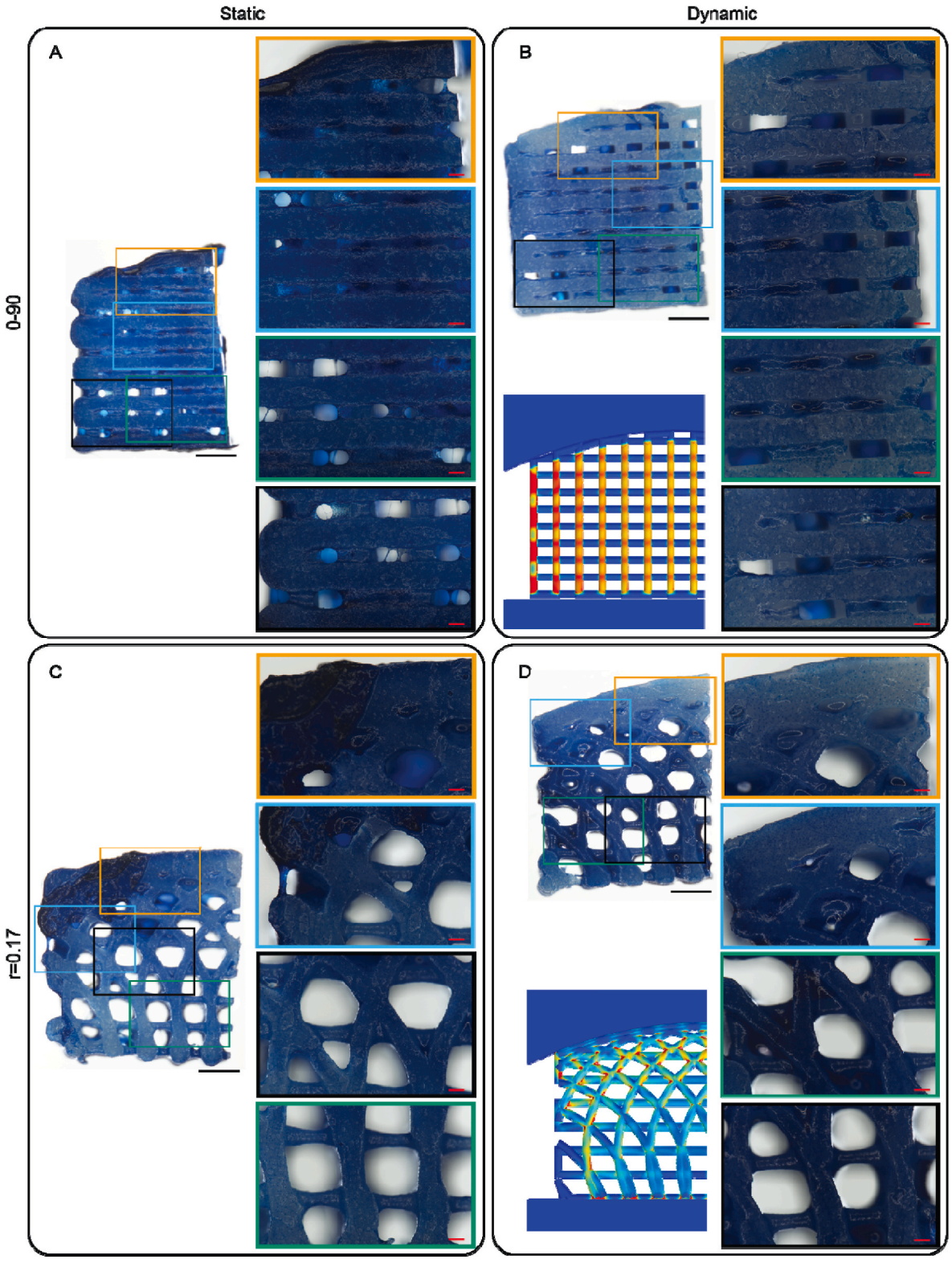

Fig. 6. Alcian blue staining of the tested scaffold after 28 days of culture. The left panels show a stained scaffold and in the right panels a close up of selected areas. A finite element model with the von Mises stress as a reference in the dynamic samples. (A) 0–90 woodpile design after static culture. (B) 0–90 woodpile design after dynamic culture. (C) r = 0.17 hypotrochoidal design after static culture. (D) r = 0.17 hypotrochoidal design after dynamic culture. Scale bar in the left panels represents 1 mm; in the close up panels 200 μm.

the collagen that was deposited in the 0–90 woodpile design was collagen type X, which is a known hypertrophic marker [42]. ATDC5 cells are known to be hypertrophic and deposit collagen type X [43]. A study by Shukunami et al. shows that collagen type X deposition starts after 21 days in 2D [44]. In our study, the collagen type X deposition was primarily deposited in the areas where the von Mises stress was the highest according to the finite element model. The fibers within the samples that were unstimulated had a lower collagen type X deposition.

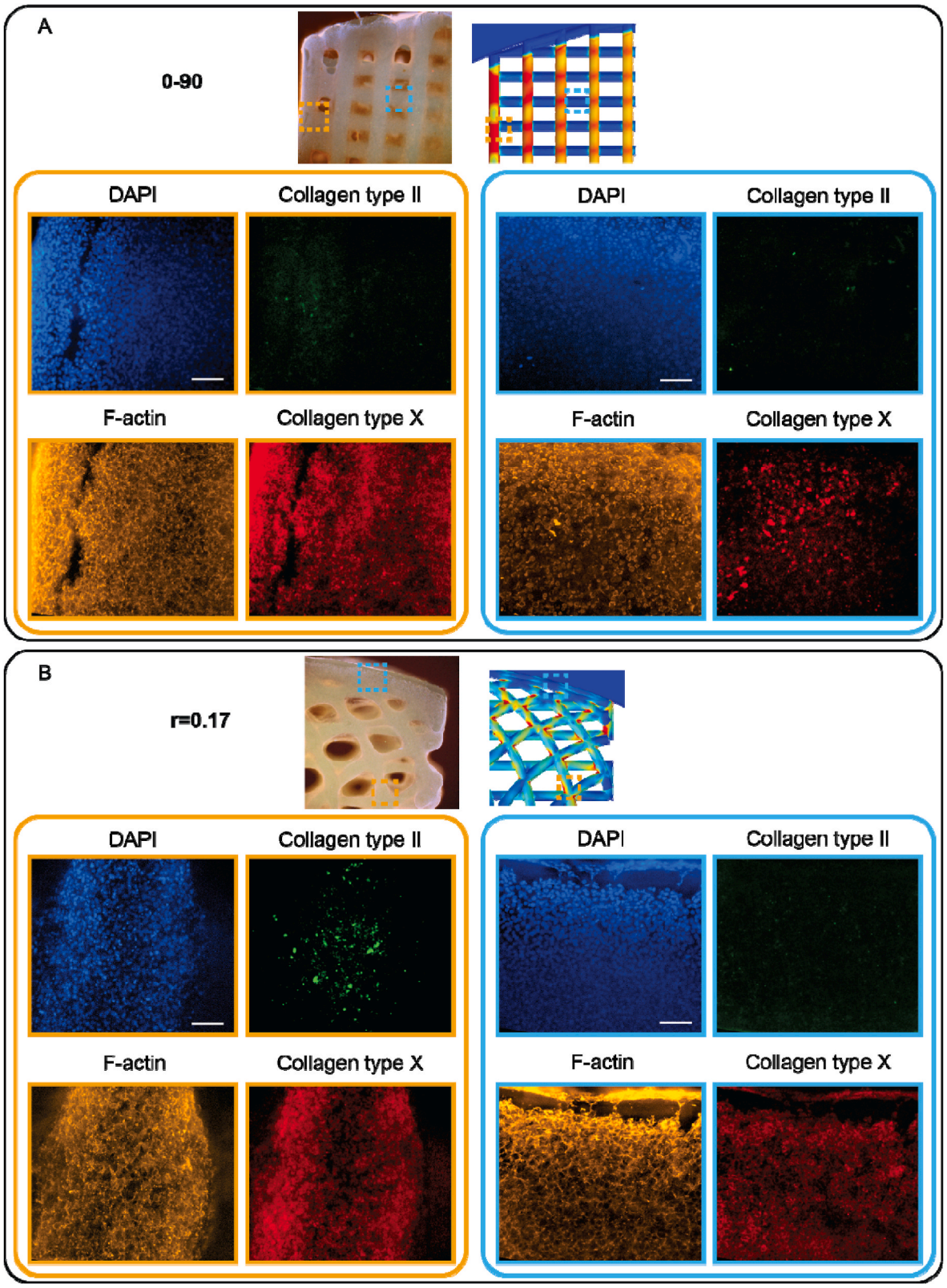

Fig. 7. Cells after 28 days in dynamic culture. On top of the panel an overview image of the scaffold with the finite element model as reference. The left panel set with orange boundaries an area with a high amount of von Mises stress and the right panel set with blue boundaries an area with a low amount of von Mises stress. (A) 0–90 woodpile design. (B) r = 0.17 hypotrochoidal design. Scale bars represent 500 μm in the overview panel and 200 μm in the close up.

Another method to decrease the amount of collagen type X is to use inhibitors such as parathyroid hormone [45] or using other polymers that showed to reduce hypertrophic differentiation [46], the latter could also enhance collagen type II production. Finally, cells that are not intrinsically hypertrophic, such as human mesenchymal stem cells (hMSCs), could serve as an alternative to reduce collagen type X [47], providing also a better route towards clinical applications. Interestingly, collagen type II expression was increased in the hypotrochoidal design, specifically in the areas where the von Mises stress were high. The von Mises stress in the hypotrochoidal design were not as high as in the 0–90 structure indicating that collagen type II deposition can be enhanced by modulating the von Mises stress. Another method to increase collagen type II deposition for this study is to extend the dynamic stimulation until 4 weeks, as was shown with primary chondrocytes [48]. Culturing the scaffolds under a lower oxygen concentration in combination with the dynamic stimulation could be an additional step that might be considered in future studies, since a lower oxygen concentration is known to improve collagen type II expression [49]. An alternative would be to change the cell type that is known to produce more collagen type II such as primary chondrocytes or mesenchymal stem cells [50]. Finally, the design is not limited to a certain material. Other less inert materials could be explored following this design.

An important aspect to note is that both the hypotrochoidal design and the 0–90 woodpile pattern contained large gaps within the scaffold. These empty gaps within the scaffolds should be filled up with ECM. A possible solutions to eliminate the gaps between the scaffolds could be to further reduce the distance between the fibers by editing the parameters of the hypotrochoidal design. An alternative could be to prolong the expansion phase of the cells on the scaffold before inducing the differentiation, or keep the scaffolds for a longer time period in culture. Finally, a more practical solution would be to start with a higher initial cell amount right before seeding them on the scaffold. In this respect, it is important to highlight that we used here a hypertrophic chondrocyte cell line to more fundamentally study the role of such arched scaffolds in modulating the local mechanical properties, and the consequent effect on chondrogenesis in dynamic cultures. When moving to more clinically applied studies, the use of MSCs would vouch for that higher ECM synthesis needed for tissue regeneration, thus filling in all the pore voids. Alternatively, these arched scaffolds could be used acellularly and be filled in by resident articular chondrogenic progenitors present in the surrounding tissue after implantation.

Generally, bundles of collagen fibers have a diameter ranging from 0.7 to 5 μm [51]. The diameter of the fibers produced in this study are two orders of magnitude bigger. Therefore, mimicking the collagen fiber arrangement could prove challenging with a technique such as FDM. However, the hypotrochoidal design could serve as a blueprint for collagen fiber deposition as collagen is synthesized intra-cellular and assembled extracellular into fibrils by chondrocytes [52]. The cells that attach to the fibers of the scaffold could start secreting pro-collagen and assemble it into collagen fibrils following the hypotrochoidal pattern. An alternative is to embed chondrocytes in a hydrogel within the hypotrochoidal design. This better represents the natural environment of chondrocytes [53]. Other techniques such as single cell acoustic patterning already allow cells to be arranged in a way that mimics the deep zone of cartilage [54]. The combination of cell patterning and having a template for the cells to follow could be worth exploring. The manufacturing of hypotrochoidal design scaffolds is not limited to FDM systems. Since the equations to generate X and Y coordinates are known, any system that uses an XY gantry could fabricate hypotrochoidal designs. Some alternative methods to produce these scaffolds might be with bioprinting or melt electrowriting systems (Fig. S12). Specifically with melt electrowriting smaller fiber diameter can be obtained reaching the diameter of the collagen fiber bundles [55]. The hypotrochoidal design could potentially be used for other tissues where a gradient occurs such as long bones [56], due to the empty inner circle in the hypotrochoid that resembles the medullary cavity and the dense outer structure resembling the compact bone (Fig. S12) [57]. Our findings indicate that the hypotrochoidal design outperformed the 0–90 woodpile design both mechanically and biologically. However, it would be interesting to determine in future studies if this effect endures *in vivo*.

4. Conclusion

Here, we introduced a hypotrochoidal design to fabricate scaffolds for cartilage tissue engineering. Such scaffolds mimic the morphological architecture of collagen fibers in articular cartilage, despite being still an order of magnitude larger than native collagen. It was shown that the hypotrochoidal design had an improved toughness compared to a 0–90 woodpile design. In addition, the stress distribution in the hypotrochoidal was improved due to the arched architecture that was introduced. The dynamic culture showed that the collagen deposition was improved and the hypotrochoidal design showed synthesis of collagen type II deposition in the specific areas of the scaffolds with a higher amount of stress and reduction of collagen type X deposition in the specific areas of the scaffolds with a lower amount of stress.

5. Materials and methods

5.1. Scaffold fabrication

Poly(ε-caprolactone) (PCL) (M_n 45.000, Sigma-Aldrich,USA) was used to fabricated scaffolds via FDM using a Bioscaffolder (SysENG, Germany). Briefly, pellets of PCL were placed in a stainless steel syringe and heated up to 110 °C. A pressure of 4 bar was used to force the molten polymer to the extrusion screw, which was set at a constant rotational speed of 45 rpm. A 25G nozzle (260 μm internal diameter) was used for extrusion. The layer thickness and speed was kept constant at 180 μm and 400 mm/min, respectively.

A custom written python script (Python Software Foundation, Version 3.7.0) was developed to generate the deposition pattern for extrusion. Using a hypotrochoidal function both X and Y coordinates were calculated (Equation (1) and Equation (2) respectively). R = the radius of the large circle, r = the radius of the rolling circle and d = the distance between the center of the rolling circle and the point which is traced. Afterwards, cut off values were set to mark the boundaries of the scaffold. The hypotrochoidal scaffold followed equation R = 10 and d = 4 with cutoff values between −5 and 5 in the X and bigger than 8 in the Y direction. As a variable parameter for the mechanical characterization, r was changed between 0.17 and 0.68. After each hypotrochoidal layer, two meandering layers that matched the outline of the scaffold were deposited with a fixed strand distance of 800 μm. The radius of this surface can be calculated with R = the radius of the large circle, r = the radius of the rolling circle and d = the distance between the center of the rolling circle and the point which is traced (Equation (3)). As control, the hypotrochoidal layer was replaced with a meandering woodpile layer of similar tool pathway length but with a 90° rotation between layers (0–90). The final scaffolds were 10 mm wide, 3 mm deep and 6 mm high at the top of the superficial zone.

$$X(\theta) = (R-r)\cos\theta + d\cos\left(\frac{R-r}{r}\theta\right) \quad (1)$$

$$Y(\theta) = (R-r)\sin\theta + d\sin\left(\frac{R-r}{r}\theta\right) \quad (2)$$

$$\textit{Superficial zone radius} = (R-r) + d \quad (3)$$

5.2. Scaffold characterization

Scaffold geometry and architecture was characterized by Stereomicroscopy (SMZ25, Nikon instruments) with a dark field illuminator (Nikon instruments). MicroCT was used to qualitatively and quantita-

tively investigate the 3D structure, volume and available surface area. The obtained micrographs were reconstructed using Nrecon software (Version 1.7.1.6., Bruker MicroCT). The scanning parameters were set as follows: 2452 × 1640 camera resolution, 6.5 μm pixel size, source voltage and current of 50 kV and 130 μA respectively, 0.2° rotation step and 4 averaged frames. Pore shape was visualised using Ctvox (Version 3.3.0r1403, Bruker MicroCT) software and the quantitative data was analysed through Ctan software (1.18.4.0+, Bruker MicroCT). The scaffold was divided in three different sections based on the three zones found in articular cartilage [20], the deep, middle and superficial zone set at 25 %, 55 % and 20 % of the scaffold, respectively. The fraction of the pore volume in each zone was derived from Equation (4).

$$Pore\ volume\ fraction = \left(1 - \frac{V_{Solid(zone)}}{V_{total}}\right) * 100\% \quad (4)$$

where $V_{solid(zone)}$ from each zone was obtained from the micro-CT analysis. V_{total} was calculated based on an equivalent solid block that was generated with computer-assisted design (CAD) (Rhino 6, Robert McNeel Associates, Version 6.19) with the dimension of the full scaffold. Moreover, for all samples the total volume of pore space (for the superficial, middle, and deep zone) was obtained by the manual selection of the region of interest (ROI) using CTAn software (version 1.18.4.0+, Bruker, Kontich, Belgium). However, these results should be carefully considered since the manual selection might include variations in each fabricated sample.

5.3. Mechanical characterization

A custom designed adapter made of aluminum was used with a matching curvature of the scaffolds to maintain full contact area of the surface during mechanical testing (ElectroForce 3230, TA instruments, USA). Compression tests were performed using a 45 N load cell (ElectroForce) and the compression rate was set at 1 % strain/s with a limit to 30 %. A camera (DMC-G3, Panasonic) with macro lens (Panagor 90 mm f2.8, Komine) was used for video acquisition during the compression test to observe the deformation. The Young's Modulus was calculated from the linear part of the stress strain curves. A pre-load of 1 N was applied before the mechanical test was initiated. The yield strain and strength were determined from the yield point that was set at the intersection between the stress-strain curve and the linear line drawn from the Young's modulus with a 0.2 % offset. The toughness of the scaffold was calculated as the area under the stress/strain curve up until the yield point. The maximum strain for the fatigue test was set at 2.5 % based on the data obtained from the compression test. During that test 100 cycles were performed with a frequency of 1 Hz. A single cycle of the hysteresis curve was plotted and the amount of energy lost per cycle was calculated as the difference in area under the curve between the loading and unloading part of the hysteresis. This was normalized against the total amount of energy to correct for differences between the scaffold designs.

5.4. Finite element modeling

A custom written script in Rhino grasshopper was used to convert the G-code of the hypotrochoidal design from the printer into a 3D CAD model. The CAD files of the tested designs were imported in finite element modeling software (COMSOL Multiphysics, COMSOL B.V. Version 6.0). The model was fixed at the bottom part and a concave fixture was made in the software to match the curvature of the scaffold. The radius of this curvature was based on equation (3). The contacts between the scaffolds and the fixture were fixed and a boundary condition was set to constrain the scaffold from falling forward during the simulation. A strain of 10 % was simulated in steps of 2 % and the Von Mises stress along with the displacement were plotted.

5.5. Cell culture

ATDC5 (RIKEN cell bank), a teratocarcinoma derived chondrogenic cell line, was used to test the effect of the hypotrochoidal design on cells. Cells were trypsinized before reaching 80 % confluence and 75.000 cells were seeded per scaffold. The cells were brought to a concentration of 2,500,000 cells/ml and a 30 μl cell suspension was dropped on the side of the scaffold. After 2 h the scaffold was flipped and after a total of 4 h of attachment, the scaffolds were transferred into Dulbecco's Modified Eagle Medium: nutrient mixture F-12 (DMEM-F12) (Sigma-Aldrich) expansion media supplemented with 5 % fetal bovine serum (FBS) (Sigma-Aldrich) and 1 % Penicillin Streptomycin (Thermo Fisher Scientific). After 1 day, the media was switched to differentiation media, which consisted of DMEM-F12 supplemented with 5 % FBS, 1 % Insuline, Transferin, sodium and Selenite (ITS) (Thermo Fisher Scientific), and 1 % Penicillin Streptomycin. After 7 days, some of the scaffolds were transferred to a custom made bioreactor for dynamic stimulation. The bioreactor was powered by a DC-motor that was powered externally by a power supply. The DC-motor rotated a camshaft with a wedge shape cam at the end. The cam pushed a block that compresses the scaffold. The strain applied on the scaffold was determined by the shape of the cam. The stimulation was performed for 2 h per day at 1 Hz and 2.5 % strain. The scaffolds were kept for a total of 28 days with media changes every other day.

5.6. Microscopy and cell analysis

Scaffolds were harvested after 28 days and used to analyze DNA, glycosaminoglycans (GAG) and collagen content or fixated for histological evaluation. A plate reader (CLARIOstar, BMG labtech) was used to quantify the biochemical assays. Scaffolds that were used for quantification were freeze/thawed 3 times before being submerged in 1 mg/ml proteinase K Tris/EDTA buffer solution. Samples were freeze/thawed again for three times after an overnight incubation at 56 °C in proteinase K solution. A part of the lysate solution was used to analyze DNA content through a DNA analysis kit (CyQUANT™ Cell Proliferation Assay Kit, Thermo Fischer Scientific) according to the manufacturer's protocol. The samples were excited at 480 nm and emission was measured at 520 nm. The amount of DNA present in the sample was calculated from a known bacteriophage λ DNA standard. Another part of the solution was used to perform a GAG assay with 1,9-dimethylmethylene blue (DMMB) (Sigma-Aldrich) dye. The absorbance was measured both at 525 nm and 595 nm. The amount of GAGs in the sample was calculated by the difference in absorbance from both wavelengths and compared to a known chondroitin sulfate standard. The final part portion of the lysate was used to quantify the collagen content according to a hydroxyproline assay (Sigma-Aldrich). The absorbance was measured at 570 nm and the collagen content in the sample was determined from a hydroxyproline standard.

The scaffolds used for microscopy were fixed with 4 % Paraformaldehyde (PFA) (VWR) for 1 h and subsequently placed in PBS until further processing. Cells were stained with 1/250 dilution (0.23 μg/ml) DAPI (Sigma-Aldrich), 1/200 (0.5 μM) Phalloidin (Thermo Fisher Scientific), 1/400 dilution Collagen type II (Anti-Collagen type II, ab34712, Abcam) and 1/200 dilution Collagen type X (Anti-Collagen type X, ab49945, Abcam). The scaffolds were stained with an Alcian blue staining (Sigma-Aldrich) with a Nuclear red counterstaining (Sigma-Aldrich) to check the presence of GAGs. Fluorescent images were taken (Nikon Eclipse Ti-e) and the bright field images were acquired with a stereomicroscope (SMZ25, Nikon instruments).

5.7. Statistics

Statistical analyses were performed with GraphPad Prism 8.1.2. Significant differences were tested using an ANOVA test with a Dunnett multiple comparisons test and a student's t-test to compare among two

groups. The tests were considered significant when $p < 0.05$.

Credit authors statement

Kenny A. van Kampen: Conceptualization, Methodology, Formal analysis, Investigation, Writing – Original Draft, Visualization. Elena Olaret: Formal analysis, Investigation, Review & Editing, Visualization. Izabela-Cristina Stancy: Resources, Writing – Review & Editing, Supervision. Daniela Duarte Campos: Resources, Writing – Review & Editing, Supervision. Horst Fischer: Resources, Writing – Review & Editing, Supervision. Carlos Mota: Coneptualization, Resources, Writing – Review & Editing, Supervision, Funding acquisition. Lorenzo Moroni: Conceptualization, Resources, Writing – Review & Editing, Supervision, Funding acquisition.

Declaration of competing interest

The authors declare that they have no known competing financial interests or personal relationships that could have appeared to influence the work reported in this paper.

Data availability

Data will be made available on request.

Acknowledgements

This work was supported by H2020 FAST (NMP-7, GA n. 685825), the ERC Cell Hybridge (GA n. 637308). The microCT analyses was supported by the European Regional Development Fund (6695072), through Competitiveness Operational Program 2014–2020, Priority axis 1, ID P_36_611, MySMIS code 107066, INOVABIOMED, Romania. IC Stancu and E Olaret acknowledge the project Integrating mechanically-tunable 3D printing with new bioactive multi(nano)materials for next functional personalized bone regenerative scaffolds, PN–III–P4-PCE-2021-1240, no. PCE 88/2022. We also gratefully acknowledge Dr. J. Fernández-Pérez for the supervision during the hydroxyproline assay, A. Chandrakar for the melt electro written scaffold, Dr. M. Decarli for the bioprinting of the hypotrochoidal scaffold.

Appendix A. Supplementary data

Supplementary data to this article can be found online at https://doi.org/10.1016/j.mtbio.2023.100830.

References

[1] J. Buckwalter, H. Mankin, J. Bone Joint Surg. 79 (1997) 600.
[2] A.J. Sophia Fox, A. Bedi, S.A. Rodeo, Sports health 1 (2009) 461.
[3] L. Sharma, N. Engl. J. Med. 384 (2021) 51.
[4] D.J. Huey, J.C. Hu, K.A. Athanasiou, Science 338 (2012) 917.
[5] H. Muir, P. Bullough, A. Maroudas, J. Bone Joint Surg. British 52 (1970) 554.
[6] M. Ulrich-Vinther, M.D. Maloney, E.M. Schwarz, R. Rosier, R.J. O'Keefe, JAAOS-J. Am. Acad. Orthopaedic Surg. 11 (2003) 421.
[7] F. Guilak, D.L. Butler, S.A. Goldstein, Clin. Orthop. Relat. Res. 391 (2001) S295.
[8] a) R.M. Aspden, D.W. Hukins, Proc. Roy. Soc. Lond. B Biol. Sci. 212 (1981) 299; b) R. Minns, F. Steven, J. Anat. 123 (1977) 437.
[9] T. Klein, B. Schumacher, T. Schmidt, K. Li, M. Voegtline, K. Masuda, E.-M. Thonar, R. Sah, Osteoarthritis Cartilage 11 (2003) 595.
[10] a) J.D. Lawrence, A Catalog of Special Plane Curves, Courier Corporation, 2013.b) M. Bouthillier, 2018.
[11] K. Nakanishi, H. Kojima, T. Watanabe, Acta Astronaut. 68 (2011) 1024.
[12] C. Goldstein, J. Gray, J. Ritter, L'Europe mathématique/Mathematical Europe: Histoires, Mythes, Identités, Les Editions de la MSH, 1996.
[13] a) B. Glisic, J. Int. Assoc. Shell and Spatial Struct. 61 (2020) 227; b) C. Zhao, Y. Liu, P. Wang, M. Jiang, J. Zhou, X. Kong, Y. Chen, F. Jin, Struct. Concr. 22 (2021) 1913.
[14] a) H.-J. Yen, C.-S. Tseng, S.-h. Hsu, C.-L. Tsai, Biomed. Microdevices 11 (2009) 615; b) M.E. Hoque, Y.L. Chuan, I. Pashby, Biopolymers 97 (2012) 83.
[15] L. Moroni, J.R. de Wijn, C.A. van Blitterswijk, Biomaterials 27 (2006) 974.
[16] a) K.-C. Hung, C.-S. Tseng, L.-G. Dai, S.-h. Hsu, Biomaterials 83 (2016) 156; b) M.A. Shamekhi, H. Mirzadeh, H. Mahdavi, A. Rabiee, D. Mohebbi-Kalhori, M. B. Eslaminejad, Int. J. Biol. Macromol. 127 (2019) 396.
[17] W. Kosorn, M. Sakulsumbat, P. Uppanan, P. Kaewkong, S. Chantaweroad, J. Jitsaard, K. Sitthiseripratip, W. Janvikul, J. Biomed. Mater. Res. B Appl. Biomater. 105 (2017) 1141.
[18] a) S.M. Bittner, B.T. Smith, L. Diaz-Gomez, C.D. Hudgins, A.J. Melchiorri, D. W. Scott, J.P. Fisher, A.G. Mikos, Acta Biomater. 90 (2019) 37; b) A. Di Luca, I. Lorenzo-Moldero, C. Mota, A. Lepedda, D. Auhl, C. Van Blitterswijk, L. Moroni, Adv. Healthcare Mater. 5 (2016) 1753.
[19] J. Baena, G. Jiménez, E. López-Ruiz, C. Antich, C. Griñán-Lisón, M. Perán, P. Gálvez-Martín, J. Marchal, Exp. Biol. Med. 244 (2019) 13.
[20] M. Uhl, C. Ihling, K. Allmann, J. Laubenberger, U. Tauer, C. Adler, M. Langer, Eur. Radiol. 8 (1998) 1123.
[21] Q.L. Loh, C. Choong, Tissue Eng. Part B: Rev. 19 (2013) 485.
[22] R. Sayles, T. Thomas, J. Anderson, I. Haslock, A. Unsworth, J. Biomech. 12 (1979) 257.
[23] P. Łuczkiewicz, K. Daszkiewicz, W. Witkowski, J. Chróścielewski, W. Zarzycki, J. Biomech. 48 (2015) 1356.
[24] S.M. McNary, K.A. Athanasiou, A.H. Reddi, Tissue Eng. 20 (2014) 921.
[25] G. Dowthwaite, A. Ward, J. Flannely, R. Suswillo, C. Flannery, C. Archer, A. Pitsillides, Matrix Biol. 18 (1999) 523.
[26] a) C. Gegg, F. Yang, Acta Biomater. 101 (2020) 196; b) W. Wei, H. Dai, Bioact. Mater. 6 (2021) 4830; c) Y. Sun, Q. Wu, Y. Zhang, K. Dai, Y. Wei, Nanomed. Nanotechnol. Biol. Med. 37 (2021), 102426.
[27] a) X. Hu, W. Li, L. Li, Y. Lu, Y. Wang, R. Parungao, S. Zheng, T. Liu, Y. Nie, H. Wang, Tissue Cell 58 (2019) 84; b) D.L. Dorcemus, H.S. Kim, S.P. Nukavarapu, Biomed. Mater. 16 (2021), 035021.
[28] S. Mohanty, L.B. Larsen, J. Trifol, P. Szabo, H.V.R. Burri, C. Canali, M. Dufva, J. Emnéus, A. Wolff, Mater. Sci. Eng. C 55 (2015) 569.
[29] S. Roberts, J.P. Urban, H. Evans, S.M. Eisenstein, Spine 21 (1996) 415.
[30] C.J. Little, N.K. Bawolin, X. Chen, Tissue Eng. Part B: Rev. 17 (2011) 213.
[31] D.E. Shepherd, B.B. Seedhom, Rheumatology 38 (1999) 124.
[32] H. Chen, Y. Liu, C. Wang, A. Zhang, B. Chen, Q. Han, J. Wang, Comput. Biol. Med. 130 (2021), 104241.
[33] J.E. Jeffrey, D.W. Gregory, R.M. Aspden, Arch. Biochem. Biophys. 322 (1995) 87.
[34] L.T. Brody, Phys. Ther. Sport 16 (2015) 301.
[35] F. Tahmasebinia, Y. Ma, K. Joshua, S.M.E. Sepasgozar, Y. Yu, J. Li, S. Sepasgozar, F. A. Marroquin, Sustainability 13 (2021) 2598.
[36] F. Malekipour, C. Whitton, D. Oetomo, P.V.S. Lee, J. Mech. Behav. Biomed. Mater. 26 (2013) 127.
[37] a) B.M. Lawless, H. Sadeghi, D.K. Temple, H. Dhaliwal, D.M. Espino, D.W. Hukins, J. Mech. Behav. Biomed. Mater. 75 (2017) 293; b) A. Weizel, T. Distler, D. Schneidereit, O. Friedrich, L. Bräuer, F. Paulsen, R. Detsch, A. Boccaccini, S. Budday, H. Seitz, Acta Biomater. 118 (2020) 113.
[38] D.D. Chan, L. Cai, K.D. Butz, S.B. Trippel, E.A. Nauman, C.P. Neu, Sci. Rep. 6 (2016), 19220.
[39] a) A. Sharma, L.D. Wood, J.B. Richardson, S. Roberts, N.J. Kuiper, Arthritis Res. Ther. 9 (2007) R79; b) T.E. Hardingham, A.J. Fosang, Faseb. J. 6 (1992) 861.
[40] P. Bansal, N.S. Joshi, V. Entezari, M. Grinstaff, B.D. Snyder, Osteoarthritis Cartilage 18 (2010) 184.
[41] S. Treppo, H. Koepp, E.C. Quan, A.A. Cole, K.E. Kuettner, A.J. Grodzinsky, J. Orthop. Res. 18 (2000) 739.
[42] G. Shen, Orthod. Craniofac. Res. 8 (2005) 11.
[43] H. Akiyama, C. Shukunami, T. Nakamura, Y. Hiraki, Cell Struct. Funct. 25 (2000) 195.
[44] C. Shukunami, K. Ishizeki, T. Atsumi, Y. Ohta, F. Suzuki, Y. Hiraki, J. Bone Miner. Res. 12 (1997) 1174.
[45] F. Mwale, G. Yao, J.A. Ouellet, A. Petit, J. Antoniou, Tissue Eng. 16 (2010) 3449.
[46] a) V. Nelea, L. Luo, C.N. Demers, J. Antoniou, A. Petit, S. Lerouge, M. R. Wertheimer, F. Mwale, Journal of biomedical materials research Part A: an Official Journal of the Society for biomaterials, Jpn. Soc. Biomater., Aust. Soc. Biomater., Korean Soc.r Biomater. 75 (2005) 216; b) S. Camarero-Espinosa, A. Calore, A. Wilbers, J. Harings, L. Moroni, Acta Biomater. 102 (2020) 192.
[47] C.N. Salinas, K.S. Anseth, Biomaterials 29 (2008) 2370.
[48] S.D. Waldman, C.G. Spiteri, M.D. Grynpas, R.M. Pilliar, R.A. Kandel, Tissue Eng. 10 (2004) 1323.
[49] a) C. Gaut, K. Sugaya, Regen. Med. 10 (2015) 665; b) V.V. Meretoja, R.L. Dahlin, S. Wright, F.K. Kasper, A.G. Mikos, Biomaterials 34 (2013) 4266.
[50] D. Bosnakovski, M. Mizuno, G. Kim, S. Takagi, M. Okumura, T. Fujinaga, Biotechnol. Bioeng. 93 (2006) 1152.
[51] a) D. MacKenna, S. Vaplon, A.D. McCULLOCH, Am. J. Physiol. Heart Circ. Physiol. 273 (1997) H1576; b) M. Kääb, I. Ap Gwynn, H. Nötzli, J. Anat. 193 (1998) 23.
[52] M.G. Patino, M.E. Neiders, S. Andreana, B. Noble, R.E. Cohen, Implant Dent. 11 (2002) 280.
[53] J. Riegger, R.E. Brenner, Int. J. Mol. Sci. 21 (2020) 1560.
[54] J.P. Armstrong, E. Pchelintseva, S. Treumuth, C. Campanella, C. Meinert, T. J. Klein, D.W. Hutmacher, B.W. Drinkwater, M.M. Stevens, Advanced Healthcare Materials, 2022, 2200481.

[55] G. Hochleitner, E. Fürsattel, R. Giesa, J. Groll, H.W. Schmidt, P.D. Dalton, Macromol. Rapid Commun. 39 (2018), 1800055.
[56] V.I. Sikavitsas, J.S. Temenoff, A.G. Mikos, Biomaterials 22 (2001) 2581.
[57] Q. Fu, E. Saiz, A.P. Tomsia, Acta Biomater. 7 (2011) 3547.